Journal of Inorganic Biochemistry 256 (2024) 112549

Contents lists available at ScienceDirect

Journal of Inorganic Biochemistry

journal homepage: www.elsevier.com/locate/jinorgbio

Synthesis, characterization and irradiation enhances anticancer activity of liposome-loaded iridium(III) complexes

Shuang Tian [a], Qianying Nie [b], Haomin Chen [a], Lijuan Liang [a], Huiyan Hu [a], Shuanghui Tang [a], Jiawan Yang [a], Yunjun Liu [a,*], Hui Yin [b,*]

[a] School of Pharmacy, Guangdong Pharmaceutical University, Guangzhou 510006, China
[b] Department of Microbiology and Immunology, Guangdong Pharmaceutical University, Guangzhou 510006, China

ARTICLE INFO

Keywords:
Iridium(III) complexes
Apoptosis
Ferroptosis
Photodynamic therapy
Western blot

ABSTRACT

Herein, we synthesized and characterized two novel iridium (III) complexes: $[Ir(bzq)_2(PPD)](PF_6)$ (4a, with bzq = deprotonated benzo[*h*]quinoline and PPD = pteridino[6,7-f][1,10]phenanthroline-11,13-diamine) and $[Ir(piq)_2(PPD)](PF_6)$ (4b, with piq = deprotonated 1-phenylisoquinoline). The anticancer efficacy of these complexes, 4a and 4b, was investigated using 3-(4,5-dimethylthiazole)-2,5-diphenltetraazolium bromide (MTT). Complex 4a exhibited no cytotoxic activity, while 4b demonstrated moderate efficacy against SGC-7901, A549, and HepG2 cancer cells. To enhance their anticancer potential, we explored two strategies: (I) light irradiation and (II) encapsulation of the complexes in liposomes, resulting in the formation of 4alip and 4blip. Both strategies significantly increased the ability of 4a, 4b to kill cancer cells. The cellular studies indicated that both the free complexes 4a, 4b and their liposomal forms 4alip and 4blip effectively inhibited cell proliferation. The cell cycle arrest analysis uncovered 4alip and 4blip arresting cell growth in the S period. Additionally, we investigated apoptosis and ferroptosis pathways, observing an increase in malondialdehyde (MDA) levels, a reduction of glutathione (GSH), a down-regulation of GPX4 (glutathione peroxidase) expression, and lipid peroxidation. The effects on mitochondrial membrane potential and intracellular Ca^{2+} concentrations were also examined, revealing that both light-activated and liposomal forms of 4alip and 4blip caused a decline in mitochondrial membrane potential and an enhancement in intracellular Ca^{2+} levels. In conclusion, these complexes and them encapsulated liposomes induce cell death through apoptosis and ferroptosis.

1. Introduction

Cancer, a malignant disease, poses a serious threat to global health due to its characteristics of uncontrolled proliferation, transformation, and metastasis. This results in high recurrence and mortality rates, making cancer a challenging medical issue worldwide [1]. In the cancer chemotherapy, a series of platinum metal drugs have been a cornerstone. Their mechanism involves binding to DNA through the aquation of Pt—Cl bonds, resulting in intracellular reduction of chloride ion concentration to approximately 20 mM [2]. However, due to the serious side-effects of cisplatin, a lot of alternative metal-based compounds have been developed. This has brought about the exploration of non-platinum metal anticancer drugs possessing distinct mechanisms of action. Notably, iridium (III) compounds have shown potential as effective anticancer agents, targeting various cellular components such as mitochondria, proteins, DNA, and lysosomes [3,4]. Recent studies have highlighted the numerous iridium (III) complexes demonstrating a prominent efficiency in restraining tumor cell growth [5–15]. on the other hand, photodynamic therapy (PDT) has been considered as another effective method to cure cancer, which uses specific light wavelengths to enhance drug efficacy. Studies by Sun and colleagues have shown that an iridium(III) complex exhibits minimal cytotoxicity (IC_{50} > 100 μM) to HepG2 cells, however, upon light irradiation (425 nm), the cytotoxicity significantly increases [16]. Similarly, Liu and team found $[Ir(piq)_2(IPPH)](PF_6)$ exhibiting non-cytotoxic y (IC_{50} > 100 μM) on A549 cells in the absence of light, whereas its cytotoxicity is markedly enhanced under illumination (IC_{50} = 0.2 ± 0.05 μM) [17]. Many photosensitizers currently undergoing clinical or pre-clinical studies predominantly affect the mitochondria and induce apoptosis via PDT [18]. Furthermore, liposomes, consisting of phospholipid and cholesterol bilayers, can encapsulate both hydrophilic and lipophilic drugs, significantly enhancing their anticancer efficacy. Our previous

* Corresponding authors.
E-mail addresses: lyjche@gdpu.edu.cn (Y. Liu), huiyin0103@gdpu.edu.cn (H. Yin).

https://doi.org/10.1016/j.jinorgbio.2024.112549
Received 24 January 2024; Received in revised form 18 March 2024; Accepted 31 March 2024
Available online 2 April 2024

studies have demonstrated that liposome-encapsulated iridium(III) complexes exhibit a strong inhibitory effect on cell growth and effectively prevent tumor growth [19–21]. Additionally, we have found iridium (III) complexes with ligands bearing -NH_2 group, and their liposome-loaded counterparts, showing significant ability to inhibit cancer cell growth [21,22]. To gain more insights into their anticancer activities, this article introduces pteridino[6,7-f][1,10]phenanthroline-11,13-diamine (PPD), featuring two -NH_2 substituent groups as a ligand, two of its iridium (III) complexes (Scheme 1): [Ir(bzq)$_2$(PPD)](PF_6) (bzq = deprotonated 2-phenylpyridine) (4a) and [Ir(piq)$_2$(PPD)](PF_6) (piq = deprotonated 1-phenylisoquinoline) (4b) were prepared and characterized. Anticancer efficiency of 4a, 4b, and their liposome-loaded forms, 4alip and 4blip, was evaluated under various conditions, including light irradiation.

2. Experimental

2.1. Materials and methods

Dimethyl sulfoxide (DMSO) and RPMI 1640 were procured from Sigma, and $IrCl_3{\cdot}3H_2O$ was obtained from the Kunming Boren Precious Metals Co.Ltd. Various cell lines including SGC-7901 (gastric cancer), B16 (melanoma), A549 (human lung cancer), HCT-116 (colon cancer), HepG2 (human hepatocellular cancer), and LO2 (normal human liver) were acquired from the Chinese Academy of Sciences (CAS) Cell Bank, Shanghai, China.

Dimethyl sulfoxide served as the solvent and tetramethylsilane (TMS) as the internal standard for conducting nuclear magnetic resonance (NMR) spectroscopy. The NMR data were gained on a Varian-500 spectrometer. Additionally, UV–Vis spectra were measured on a Shimadu UV-3101PC spectrophotometer. Molecular weights of the synthesized compounds were precisely examined using high-resolution mass spectrometry (HRMS).

2.2. Synthesis of complexes 4a and 4b

2.2.1. Synthesis of [Ir(bzq)$_2$(PPD)](PF_6) (4a)

Cis-[Ir(bzq)$_2$Cl]$_2$ (0.233 g, 0.20 mmol) [23] and PPD (0.126 g, 0.40 mmol) [24] were dissolved in 28 mL CH_2Cl_2 and 14 mL CH_3OH. This solution was refluxed at 40 °C under an argon atmosphere. After 6 h, the solution was cooled and saturated aqueous NH_4PF_6 was added, the above solution was stirred for an additional 2 h. This process resulted in the formation of a distinct yellow precipitate. The crude product was subsequently purified using neutral alumina column chromatography, CH_2Cl_2-CH_3CH_2OH (*v*/v, 5:1) was employed as the eluent, collecting the yellow band, finally a yellow powder was gained. Yield: 82%. Anal calcd for $C_{42}H_{26}N_{10}PF_6Ir$: C, 50.05; H, 2.60; N, 13.90%. Found: C, 50.20; H, 2.42; N, 13.76%. ^{1}H NMR (DMSO-d_6, 500 MHz, Fig. S1, SI): δ 9.92 (d, J = 8.0 Hz, 1H), 9.47 (d, J = 7.5 Hz, 1H), 8.75 (s, 1H), 8.55 (d, J = 8.0 Hz, 2H), 8.29–8.24 (m, 3H), 8.13–8.09 (m, 4H), 8.00 (d, J = 8.5 Hz, 4H), 7.90 (d, J = 9.0 Hz, 2H), 7.60 (d, J = 5.0 Hz, 2H), 7.51–7.48 (m, 2H), 7.24 (t, J = 7.5 Hz, 2H), 6.33 (d, J = 7.5 Hz, 2H). ^{13}C NMR (DMSO-d_6, 125 MHz, Fig. S2, SI): 172.48, 164.92, 163.40, 156.76, 156.10, 152.80, 150.93, 149.77, 147.66, 147.16, 144.43, 140.82, 138.08, 135.76, 135.19, 134.23, 132.92, 131.36, 130.50, 130.18, 129.93, 129.02, 128.36, 127.15, 126.29, 124.72, 123.26, 120.90. HRMS (CH_3CH_2OH): m/z = 863.1915 ([M – PF_6])$^+$.

2.2.2. Synthesis of [Ir(piq)$_2$(PPD)](PF_6) (4b)

This compound was obtained with the same method described for 4a with [Ir(piq)$_2$Cl]$_2$ [23] in place of [Ir(bzq)$_2$Cl]$_2$. Yield: 80%. Anal calcd for $C_{46}H_{30}N_{10}PF_6Ir$: C, 50.12; H, 2.85; N, 13.21%. Found: C, 50.33; H, 2.97; N, 13.38%. ^{1}H NMR (DMSO-d_6, 500 MHz, Fig. S3, SI): δ 9.97 (dd, J = 1.5, J = 7.5 Hz, 1H), 9.55 (dd, J = 2.0, J = 8.0 Hz, 1H), 9.06–9.01 (m, 2H), 8.77 (s, 1H), 8.42 (d, J = 8.5 Hz, 2H), 8.30 (s, 1H), 8.15–8.05 (m, 6H), 7.98 (dd, J = 1.5, J = 5.0 Hz, 1H), 7.92–7.87 (m, 5H), 7.54–7.48 (m, 4H), 7.19 (t, J = 8.0 Hz, 2H), 6.98 (t, J = 7.5 Hz, 2H), 6.27 (d, J = 8.5 Hz, 2H). ^{13}C NMR (DMSO-d_6, 125 MHz, Fig. S4, SI): 172.49, 168.27, 164.95, 163.43, 162.80, 156.16, 153.77, 152.22, 150.35, 149.73, 147.08, 145.88, 144.50, 141.63, 137.03, 135.91, 135.31, 132.99, 132.53, 132.11, 131.51, 131.05, 130.66, 129.85, 128.43, 128.18, 126.91, 126.35, 125.99, 122.89, 122.66. HRMS (CH_3CH_2OH): m/z = 915.1718 ([M – PF_6])$^+$.

2.3. Determination of purity of 4a and 4b

The purity of the synthesized 4a and 4b was detected using HPLC at room temperature. The mobile phases A and B consisted of H_2O with 0.1% trifluoroacetic acid (TFA) and CH_3OH with 0.1% TFA, respectively. The flow rate was maintained at 3 mL/min. The volume ratios of H_2O to MeOH are 6:94 and 2:98 for 4a and 4b, respectively. Detection of the complexes was conducted at a wavelength of 254 nm.

2.4. Preparation of 4alip and 4blip

The liposomal forms of complexes 4a and 4b, designated as 4alip and 4blip, were synthesized using a modified reverse-phase evaporation method [25]. Initially, 4a or 4b, egg yolk lecithin (PC-98 T), cholesterol

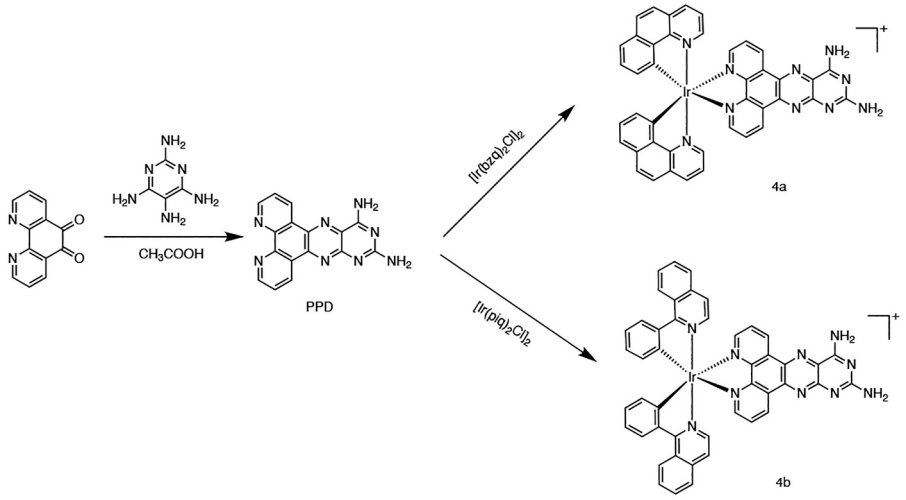

Scheme 1. Synthesis of PPD and 4a and 4b.

(CHO-HP), and DSPE-MPEG 2000 in a weight ratio of 1:30:10:10 (*w*/w) were combined in a 20 mL vial. These components were dissolved in 8 mL of chloroform (6 mL) and H_2O (2 mL). The mixture was sonicated for 5 min, then removing the organic phase, the residue was rehydrated with PBS and subjected to vortex mixing for 30 min at 45 °C. The final step involved ultrasonication and centrifugation to yield a clear, transparent liposome preparation.

2.5. Characterization of 4alip and 4blip

The zeta potentials and particle sizes of both 4alip and 4blip were determined using a laser particle sizer. To gain encapsulation efficiency, the liposomes were first centrifuged and a clear supernatant was obtained. The liposomes were then disrupted with methanol, and then measuring the absorbance at 254 nm. The concentration of 4a and 4b in the solution was determined based on a pre-established standard curve.

The encapsulation efficiency (EE%) of 4alip and 4blip was gained:

$$\mathrm{EE}\ (\%) = \frac{W_{encapsulated}}{W_{total}} \times 100\%.$$

In this equation, $W_{encapsulated}$ is the drug-loaded content detected in the supernatant after centrifugation, and W_{total} is the weight of 4a or 4b in the preparation of 4alip and 4blip.

2.6. Release examination

The release profiles of 4a and 4b from their respective liposomal suspensions, 4alip and 4blip, were determined using a dialysis method previously described in literature [26]. In this procedure, 5 mL of either 4alip or 4blip suspension, containing 1 mg of 4a or 4b, was enclosed in a dialysis bag (8–14 kDa). This setup was then immersed in 25 mL of PBS at 37 °C, with Tween 80 (0.5%, *w/v*) in a beaker. At specified time intervals, a 3.5 mL sample of the dialysate was removed for analysis, and an equivalent volume of fresh buffer was added into the beaker to maintain constant volume. The concentration of 4a or 4b in the dialysate was quantitatively assessed using a UV–Visible spectrophotometer. From these measurements, the cumulative amount of each compound released from the liposomes was calculated. The resulting data were used to plot release curves, representing the cumulative release concentration of 4a or 4b against time.

2.7. Singlet oxygen detection

The singlet oxygen $^1O_2$ was determined by UV–Vis spectra. A mixture solution of DPBF (40 μM) and 4a or 4b (10 μM) was irradiated with white light (LED lamp, 460 nm, 7.03 J/cm^2) in the different time, the absorption of DPBF (417 nm) was measured. $[Ru(bpy)_3]^{2+}$ was used as a reference. The quantum yield Φ were gained based on the Eq. [27]:

$$\Phi_{\mathrm{sample}} = \Phi_{\mathrm{Ref}} \times \left(K_{\mathrm{sample}}/K_{\mathrm{Ref}}\right) \times \left(F_{\mathrm{Ref}}/F_{\mathrm{sample}}\right)$$

K is the slope, F is calibration factor of the absorbance, $F = 1–10^{-OD}$ (OD is the absorbance of the photosensitizer at the light source wavelength).

2.8. Cell viability and IC_{50} determination

3-(4,5-dimethylthiazole)-2,5-diphenyltetraazolium bromide (MTT) assay [28] was employed to determine the cell viability and half-maximal inhibitory concentration (IC_{50}) values. The cancer cells (8×10^3 cells per well) were seeded in 96-well microassay culture plates overnight at 37 °C in a 5% CO_2 atmosphere. Various concentrations of the test complex, dissolved in DMSO, were added to the above wells. The control wells received 100 μL of culture medium without the test compound. The plates were incubated for 48 h at 37 °C in a 5% CO_2 atmosphere. After incubation, 20 μL of MTT dye solution (5 mg/mL) was added to each well. After 4 h, the MTT formazan product was dissolved with a solution (100 μL) containing 50% dimethylformamide and 20% sodium dodecyl sulfate, the optical density was measured at 490 nm.

IC_{50} values were gained by plotting the percentage of viable cells against the logarithm of the concentration and determining the concentration corresponding to 50% cell viability. Each experiment was performed in triplicate. The cell viability was calculated according to the equation:

$$\text{Cell viability}\% = \left(\left(A_{\mathrm{sample}} - A_{\mathrm{medium\ control}}\right)/\left(A_{\mathrm{cell\ control}} - A_{\mathrm{medium\ control}}\right)\right) \times 100$$

Whereas A_{sample}, A_{medium} and A_{blank} are the absorbance values of sample, medium and control.

2.9. Cell colony experiment

SGC-7901 cells were co-incubated with the compounds 4a, 4b, and their liposomal formulations, 4alip and 4blip, at their respective IC_{50} concentrations, throughout this period, the culture medium was refreshed daily. After one week, the cells were washed and fixed with paraformaldehyde. Finally, the crystal violet-stained SGC-7901 cells were photographed to observe the cell morphology and proliferation.

2.10. Cell cycle determination

Cells of SGC-7901 were co-cultured with 4a, 4b, 4alip, and 4blip (IC_{50} concentration) for 24 h. Afterwards, washing three times with PBS, the cells were fixed with 70% CH_3CH_2OH and stored at 4 °C overnight. Then the cells were again washed with PBS and stained with propidium iodide (PI). Finally, the cells were analyzed with FACS Calibur flow cytometry.

2.11. Apoptosis studies

After exposure to IC_{50} concentration of 4a, 4b, 4alip, 4blip for 24 h, SGC-7901 cells were washed with PBS three times and dyed with 200 μL Annexin V-FITC solution (25 μg/mL Annexin V-FITC, 2.5 μg/mL propidium iodide (PI), the percentage of the cell in the living, early and late apoptosis was measured with flow cytometry.

2.12. Change of the mitochondrial membrane potential

After seeded in 12-well plate overnight, SGC-7901 cells were exposed to IC_{50} concentrations of 4a, 4b, 4alip, 4blip for 24 h. Next, SGC-7901 cells were washed with PBS three times, the cells were dyed with 1 μg/mL of JC-1 (5,5′,6,6′-tetrachloro-1,1′,3,3′-tetraethyl-imidacarbocyanineiodide) for 30 min. Then the cells were washed twice with PBS and observed.

2.13. Ferroptosis studies

2.13.1. Intracellular lipid peroxidation

SGC-7901 cells were treated with IC_{50} concentrations of 4a, 4b, 4alip, and 4blip for a period of 24 h. Afterwards, the residual compounds were removed through washing the cells three times using PBS solution. As a lipid peroxidation sensor, C11-BODIPY 581/591 (2.0 μM) was applied to dye the cells for 30 min. C11-BODIPY 581/591 is commonly used to detect oxidative stress in cells, which is a crucial parameter in understanding the cellular impact of treatments. The stained cells were then photographed. The imaging was conducted at specific excitation (λ_{ex}) and emission (λ_{em}) wavelengths to detect the fluorescence of C11-BODIPY (λ_{ex} = 488 nm, λ_{em} = 510 nm for green, λ_{ex} = 581 nm, λ_{em} = 591 nm for red). This imaging approach enables the visualization of lipid peroxidation within the cells, providing valuable insights into the oxidative stress.

2.13.2. Intracellular MDA concentration

SGC-7901 cells were co-incubated with 4a, 4b, 4alip, and 4blip (IC_{50} concentrations) for 24 h. After incubation, the cells were washed twice with PBS to remove any residual treatment agents. The cells were then lysed using Radio-Immunoprecipitation Assay (RIPA) buffer, a process which helps in breaking down the cell membranes and releasing the cellular contents. The lysates were centrifuged at 4 °C for 20 min. This step allows for the separation of the soluble supernatant containing proteins from the cell debris. The supernatant was then collected for further analysis. Bicinchoninic Acid (BCA) protein assay was applied to measure the total protein concentration in each sample. Based on these concentrations, the proteins were normalized for subsequent analysis. Next, following the protocol outlined in the Lipid Peroxidation MDA assay kit, we determined malondialdehyde (MDA) content. MDA is a marker for oxidative stress and lipid peroxidation within cells. The MDA contents were determined with multimode microplate readers at 532 nm.

2.13.3. GSH content determination

After a 24-h incubation of SGC-7901 cells with 4a, 4b, 4alip and 4blip, the cells were digested, centrifuged, and collected in EP pipes. A protein removal reagent was then added to the EP pipes, and the contents were thoroughly mixed. The eppendorf tubes underwent two rapid freeze-thaw cycles, followed by a 5-min refrigeration at 4 °C. The pipes were then centrifuged for 15 min. The resulting supernatant was carefully transferred from the EP pipes to a 96-well plate. Subsequently, Glutathione (GSH) Removal Aid and GSH Removal Solution were added to the wells, and the plate was incubated at 25 °C for 60 min. Following the preparation of reagents as per the instructions of the GSH assay kit, the samples in the 96-well plate were mixed well and incubated for an additional 5 min. After this incubation, 50 μL of NADPH solution (0.5 mg/mL) was added to each well. The absorbance was measured at 412 nm.

2.14. Expression of apoptosis-related protein

Treatment of SGC-7901 cells with 4a, 4b, 4alip and 4blip for 24 h, the concentration of protein in the supernatant was obtained according to BCA (bicinchoninic acid) assay. In the sodium dodecyl sulfate-polyacrylamide gel electrophoresis, amount of the proteins in the per lane is equal. After gel electrophoresis, the gels were transferred to polyvinylidene difluoride membranes (Millipore) and blocked with 5% non-fat milk in TBST (20 mM Tris-HCl, 150 mM NaCl, 0.05% Tween 20, pH 8.0) buffer for 3 h. After washing four times with TBST buffer, the membranes were incubated with primary antibody solution at 4 °C overnight, washing four times again, the secondary antibodies were then conjugated with horseradish peroxidase (1:5000 dilution) for 70 min at room temperature. Finally, the blots were treated with the Amersham ECL Plus western blotting detection reagents.

2.15. Data analysis

The data in the study were reported as the mean ± standard deviation (SD). *t*-test was utilized to evaluate the differences between groups. $^{*}p < 0.05$ indicates a statistical difference.

3. Results and discussion

3.1. Synthesis and characterization

PPD was synthesized via condensation of 1,10-phenanthroline-5,6-dione with 2,4,5,6-tetraaminopyrimidine sulfate, following the method delineated in existing literature [24]. Complexes 4a and 4b were synthesized through reaction of $[Ir(bzq)_2Cl]_2$ or $[Ir(piq)_2Cl]_2$ with PPD. Characterization of these complexes was conducted using HRMS, ^1H NMR, and ^{13}C NMR spectra. HRMS spectra revealed molecular weights congruent with theoretical calculations. In the ^{13}C NMR spectra, the observed peaks at 172.48 and 164.92 ppm for 4a, and 172.49 and 168.27 ppm for 4b, correspond to the carbon atoms bonded to the $-NH_2$ groups.

UV–Vis spectra was applied to examine the stability of complexes 4a or 4b, as shown in Fig. S5a (SI), At 0 and 24 h, the peak shapes for 4a and 4b are the same, indicating a stable existence of 4a or 4b. Additionally, the stability of 4a was also determined using HRMS spectra, as shown in Fig. S5b (SI), the determined molecular weights are the same upon irradiation as that in the dark at 0 h and 48 h, which further affirms that the complexes are stable.

As depicted in Fig. S5c (SI), during a 20-min analysis period, a singular peak was observed for each complex, confirming their purity at 97.8% and 96.4% for 4a and 4b.

Particle sizes of 4alip and 4blip were examined using dynamic light scattering (DLS), revealing average sizes of 85.8 ± 1.7 nm for 4alip and 80.9 ± 0.8 nm for 4blip (Fig. S5d, SI). The zeta potentials of −7.09 mV for 4alip and − 12.09 mV for 4blip suggest a moderate electrostatic repulsion between particles, contributing to suspension stability and resistance to agglomeration [29]. The morphology of 4alip was examined by *transmission* electron microscope (TEM), as found from Fig. S5e (SI), 4alip displays a spherical particle size.

Encapsulation efficiency (EE%) was found to be 89.94% for 4alip and 85.42% for 4blip. Release kinetics, as shown in Fig. S5f (SI), indicated initial release concentrations of 29.1% and 15.2% within the first 0.5 h for 4alip and 4blip, respectively. Cumulative 24-h release of free 4a and 4b reached 48.7% and 46.5%, respectively, demonstrating a controlled release profile.

3.2. Cell viability and IC_{50} determination

The cytotoxic efficacy of 4a, 4b, 4alip, and 4blip toward cancer cells SGC-7901 and A549 was assessed using the 3-(4,5-dimethylthiazole)-2,5-diphenyltetrazolium bromide (MTT) assay. We employed two strategies to enhance the anticancer efficacy of 4a and 4b: (I) light irradiation and (II) encapsulation within liposomes. Fig. 1a (I) and (II) display the results of treating SGC-7901 cancer cells with varying amounts of 4a and 4b for 48 h, 4b demonstrated a moderate ability to inhibit cell proliferation, whereas 4a exhibited a weaker effect on killing cancer cells. Further experiments involved a 4-h treatment of SGC-7901 cells with 4a and 4b, followed by 30 min of light irradiation (65 w LED lamp, light dose of 7.03 $J{\cdot}cm^{-2}$, $\lambda = 460$ nm). Post-irradiation, the cell viability reduced compared to non-irradiated controls (Fig. 1a (III) and (IV)). This indicates that light irradiation enhances the cytotoxic effects of the complexes. To optimize the anticancer potential, 4a and 4b were encapsulated into liposomes, creating 4alip and 4blip. Fig. 1a (V-VIII) illustrate the enhanced inhibitory effects of 4alip and 4blip on SGC-7901 cells, both with and without irradiation. These liposome-encapsulated complexes demonstrated superior cytotoxicity compared to their non-encapsulated counterparts.

The IC_{50} values ranged from 84.1 ± 2.1 to 2.4 ± 0.2 μM (Table 1), 4a shows non-cytotoxic toward SGC-7901, A549 cells ($IC_{50} > 100$ μM), the cytotoxic activity of 4a and 4b is lower than cisplatin in the dark. However, under light irradiation, the anticancer efficacy of 4a and 4b significantly enhanced, while IC_{50} values of 4alip and 4blip toward SGC-7901 cells under light irradiation are 4.1 ± 0.2 and 2.4 ± 0.2 μM. The cytotoxic activity of 4a and 4b toward SGC-7901 cells is higher than that of complex $[Ir(bzq)_2(DIPH)](PF_6)$ (IC_{50} = 4.7 ± 0.2 μM) [19], comparable to the complex $[Ir(bzq)_2(NDPPZ)](PF_6)$ (IC_{50} = 1.6 ± 0.3 μM) [30], but lower than that of $[Ir(piq)_2(NDPPZ)](PF_6)$ (IC_{50} = 0.8 ± 0.1 μM, NDPPZ = 11-nitrodipyrido[3,2-*a*:2′,3′-*c*]phenazine) [30] and $[Ir(piq)_2(dmdppz)](PF_6)$ (IC_{50} = 0.6 ± 0.2 μM, dmdppz = 5,8-dimethoxylpyrido[3,2-*a*:2′,3′-*c*]phenazine) [31]. Generally, upon light irradiation, the compounds elevate reactive oxygen species (ROS) and $^1O_2$, while ROS and $^1O_2$ are able to quickly act with adjacent biomolecules, further disturbing the functions of normal cell, finally triggering cell

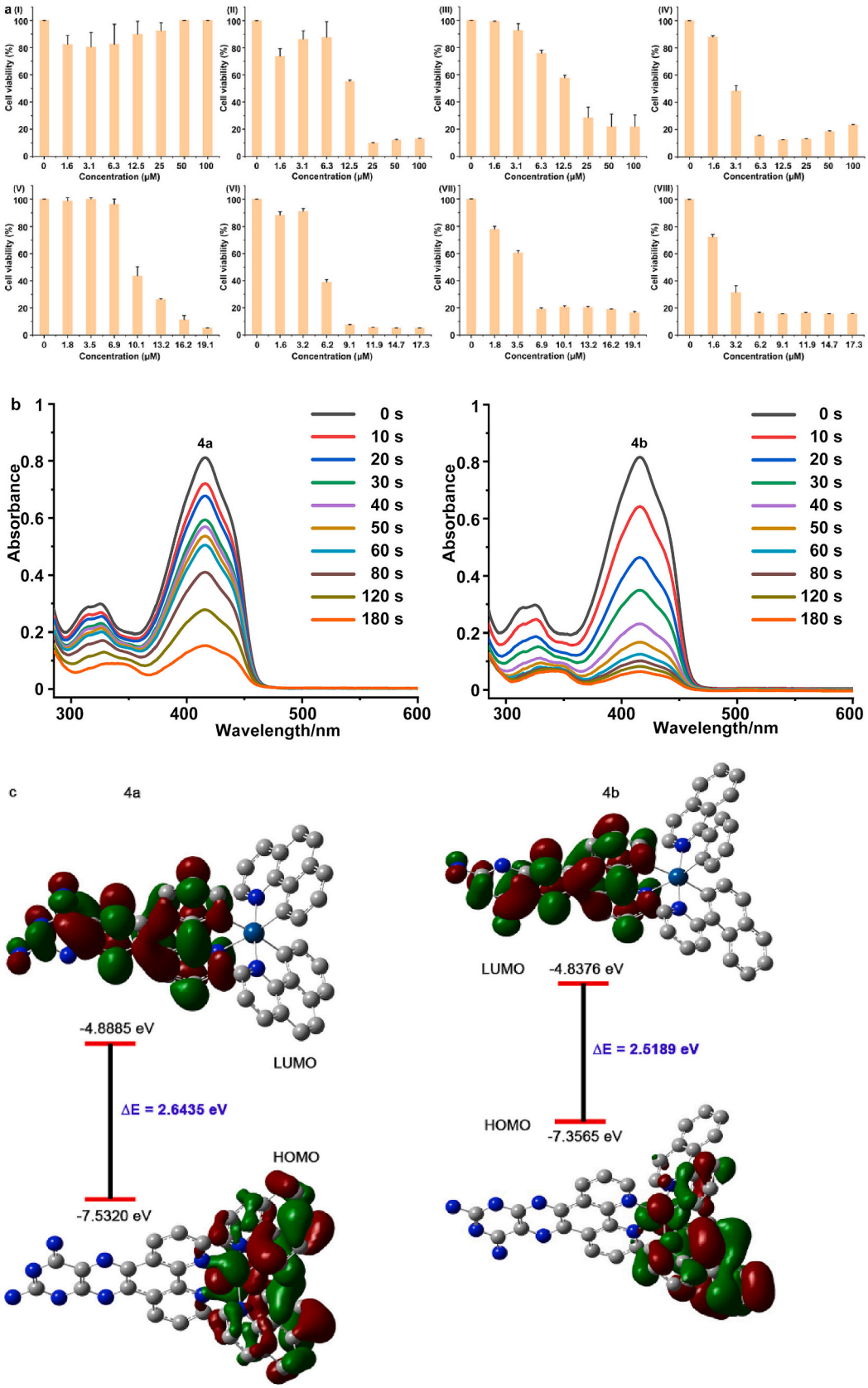

Fig. 1. (a) Cell viability of SGC-7901 cells treated with different concentrations of 4a (I) and 4b (II) (without light), 4a (III) and 4b (IV) upon light irradiation, 4alip (V) and 4blip (VI) without light, 4alip (VII) and 4blip (VIII) upon light irradiation, (b) photocatalytic oxidation of DPBF (40 μM) under white light in the presence of 10 μM of 4a and 4b in DMSO. (c) Frontier orbital energy levels and electron cloud distribution of 4a and 4b.

Note: In all the following cell experiments, 4a (light), 4b (light), 4alip (light) and 4blip (light) stand for a 4-h treatment of SGC-7901 cells with 4a, 4b, 4alip, 4blip, followed by 30 min of light irradiation (65 w LED lamp, light dose of 7.03 J·cm^{-2}, λ = 460 nm).

Table 1
IC_{50} (μM) value of complexes and their liposomes with (without) light irradiation toward selected cancer cells for 48 h.

complex	SGC-7901			A549			LO2		
	IC_{50dark}	$IC_{50light}$	PI	IC_{50} (dark)	IC_{50} (light)	PI	IC_{50} (dark)	IC_{50} (light)	PI
4a	> 100	18.0 ± 1.6		> 100	84.1 ± 2.1		> 100	> 100	
4b	11.3 ± 0.2	3.2 ± 0.2	3.5	10.5 ± 1.2	9.1 ± 1.5	1.2	52.9 ± 1.8	29.2 ± 4.1	1.8
4alip	10.5 ± 0.5	4.1 ± 0.2	2.6	34.1 ± 2.7	8.7 ± 0.2	3.9	54.9 ± 0.8	8.9 ± 0.4	6.2
4blip	5.0 ± 0.1	2.4 ± 0.2	2.1	9.7 ± 1.2	4.3 ± 0.1	2.3	29.4 ± 2.6	4.9 ± 0.3	6.0
Cisplatin	3.4 ± 0.5			5.8 ± 0.4			17.8 ± 2.5		

demise [32,33]. Based on the literature [17,34,35], we consider that 4a and 4b can validly activate $^3O_2$ to produce $^1O_2$, which makes them highly validly photosensitizers in photodynamic therapy (PDT). To confirm the production of $^1O_2$ under light irradiation, we used 1,3-diphenylisobenzofuran (DPBF) as a $^1O_2$ scavenger, see from Fig. 1b, with increase of light irradiation time, absorbance of DPBF at 417 nm reduced, indicating an increase of $^1O_2$. The quantum yields of 4a and 4b were detected with $[Ru(bpy)_3]^{2+}$ as a reference ($\Phi = 0.81$, methanol) [36]. The quantum yields of 4a and 4b was calculated to be 0.51 and 0.66, which indicates that 4b can generate $^1O_2$ more efficiently than 4a. Notably, the anticancer efficacy of 4b is higher than those of 4a against the selected cancer cells, this is line with those quantum yields. Additionally, we also calculated the energy gap between the highest occupied orbital (HOMO) and the lowest unoccupied orbital (LUMO) by DFT/B3LYP/6-31G(d, p)(C, H, N)/SDD(Ir). The size of the band gap between LUMO-HOMO of a molecule is closely related to its chemical activity. A larger HOMO-LUMO band gap will result in difficult deformation of the electron cloud, lower reactivity, and poorer anticancer activity [37,38]. As shown in Fig. 1c, the ΔE values for 4a and 4b are 2.6435 eV and 2.5189 eV, The ΔE value for 4a is larger than that of 4b, indicating that the cytotoxic activity of 4a is lower than those of 4b, which is line with the trend of antiproliferative activity of these complexes. The 4alip and 4blip exhibited higher cytotoxic activity against SGC-7901 cells than against A549 cells, therefore, SGC-7901 cells were selected for subsequent experimental analyses.

To clarify the difference of 4a, 4alip, 4b, 4blip in the cytotoxicity activity, we used flow cytometry to determine the cellular uptake, as shown Fig. S6 (SI), 4a shows low green fluorescence, the green fluorescence follows the order of 4blip > 4alip > 4b > 4a, therefore, 4a shows the lowest cytotoxic activity. In addition, inductively coupled plasma mass spectrometry (ICP-MS) was used to quantitatively measure the uptaken amounts of 4b and 4blip, after 4 h co-incubation of SGC-7901 cells with 4b (10.0 μM) and 4blip (10.0 μM), the cellular uptaken amounts for 4b and 4blip are 72.47 and 79.74 ng/10^6 cells. Hence, the uptaken amount of 4blip is more than that of 4b, this is consistent with the cytotoxic activity.

PI: phototoxicity index = $IC_{50(dark)}/IC_{50(light)}$

3.3. Cell colony and cell cycle distribution studies

Cell colony formation assays are instrumental in further evaluating the efficacy of complexes on inhibiting cell growth. Metastasis, a

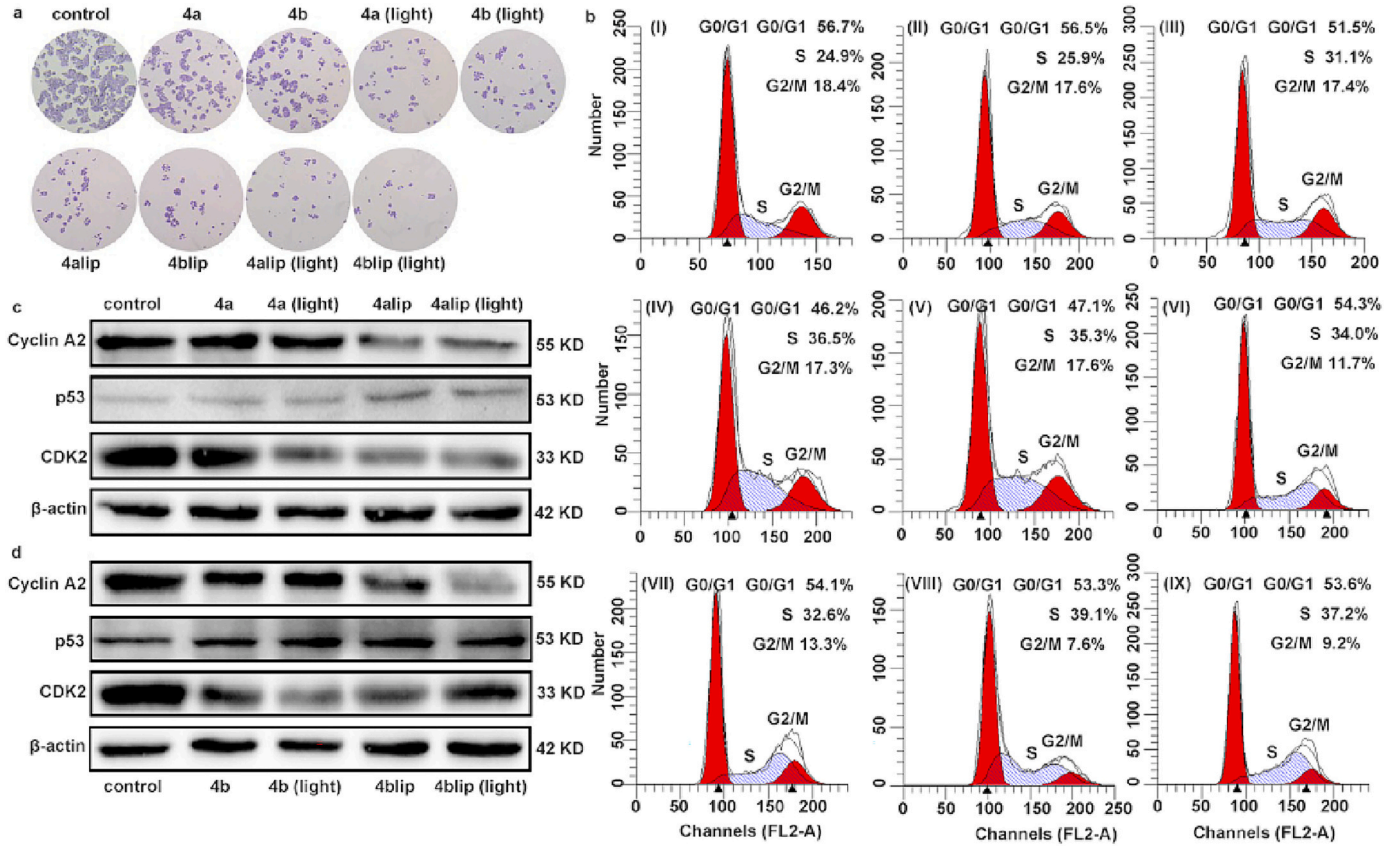

Fig. 2. (a) cell colony, (b) cell cycle arrest, (c) and (d) expression of cycle-related proteins while a 24 h treatment of SGC-7901 cells with IC_{50} concentration of 4a, 4b, 4alip, 4blip upon irradiation or without.

primary cause of cancer mortality, involves the diffusion of cancer cells from the initial site to other organs, posing a significant challenge in cancer therapy [39]. Fig. 2a indicates that complexes 4a and 4b, in their basic form, exhibit limited efficacy in inhibiting cell proliferation. However, their effectiveness is markedly enhanced upon light irradiation or encapsulation in liposomes, as both 4a, 4b and their liposomal forms 4alip, 4blip show substantial efficacy in inhibiting cell proliferation.

The cell cycle, a critical process for cell division and proliferation, offers insights into cancer mechanisms and treatment strategies. As depicted in Fig. 2b, complex 4a (II) induced minor changes in SGC-7901 cell distribution across G0/G1, S, and G2/M phases. In contrast, when SGC-7901 cells (I) were incubated for 24 h with IC_{50} concentrations of 4b (III), 4a (IV, light), 4b (V, light), 4alip (VI), 4blip (VII), 4alip (VIII, light), and 4blip (IX, light), notable increases were observed in the S phase: 6.2% for 4b, 11.6% for 4a (light), 10.4% for 4b (light), 9.1% for 4alip, 7.7% for 4blip, 14.2% for 4alip (light), and 12.3% for 4blip (light). This data suggests that these complexes inhibit cell proliferation primarily during the S phase, particularly upon light irradiation.

Cyclin A2, a pivotal protein in the cell cycle, is crucial for regulating the G1/S and G2/M phases, playing an important role in DNA replication, transcription, and tumor progression. To unravel the underlying mechanisms of these complexes and their liposomal forms in hindering cell growth, the study examined the expression of cyclin A2, p53, and CDK4. Fig. 2c and d show that 4a, 4b, 4alip, and 4blip downregulated cyclin A2 and CDK4 expression while upregulating p53 protein levels. Therefore, these complexes and their liposomal forms inhibit cell growth during S phase through modulating cyclin A2, p53, and CDK4 expression.

3.4. Superoxide anion, mitochondrial membrane potential, cytochrome c, apoptosis

ROS play an important role in cancer cell death and apoptosis, it

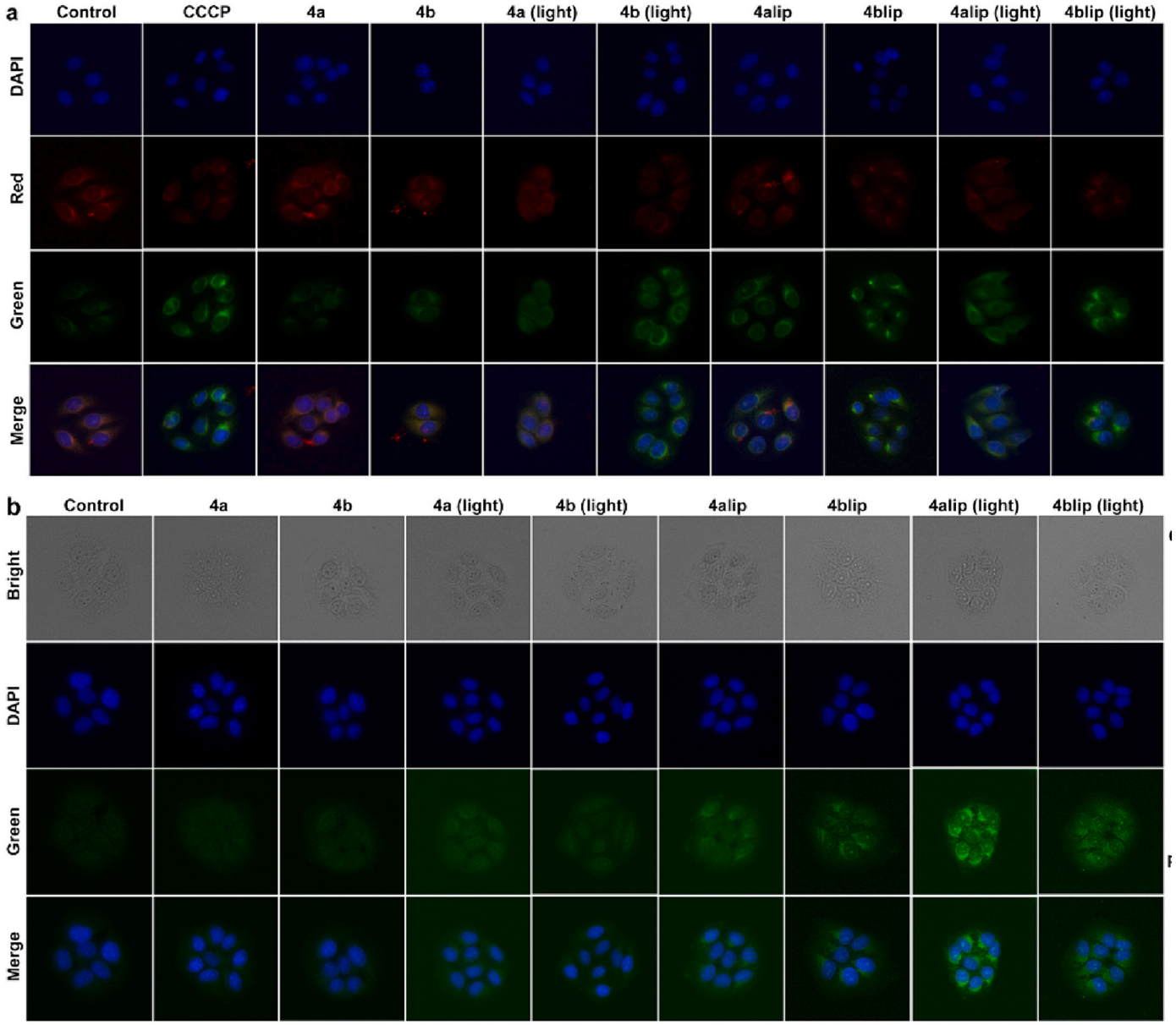

Fig. 3. (a) Detection of the change of mitochondrial membrane potential, (b) release of cytochrome *c*, (c) apoptosis (Q2, Q3, Q4 representing late, early and living cells), SGC-7901 cells (I) treated with 4a (II), 4a (light) (IV), 4alip (VI) 4alip (light, VIII), 4b (III), 4b (light) (V), 4blip (VII), and 4blip (light) (IX). (d and f) expression of apoptosis-related proteins, (e and g) gray values.

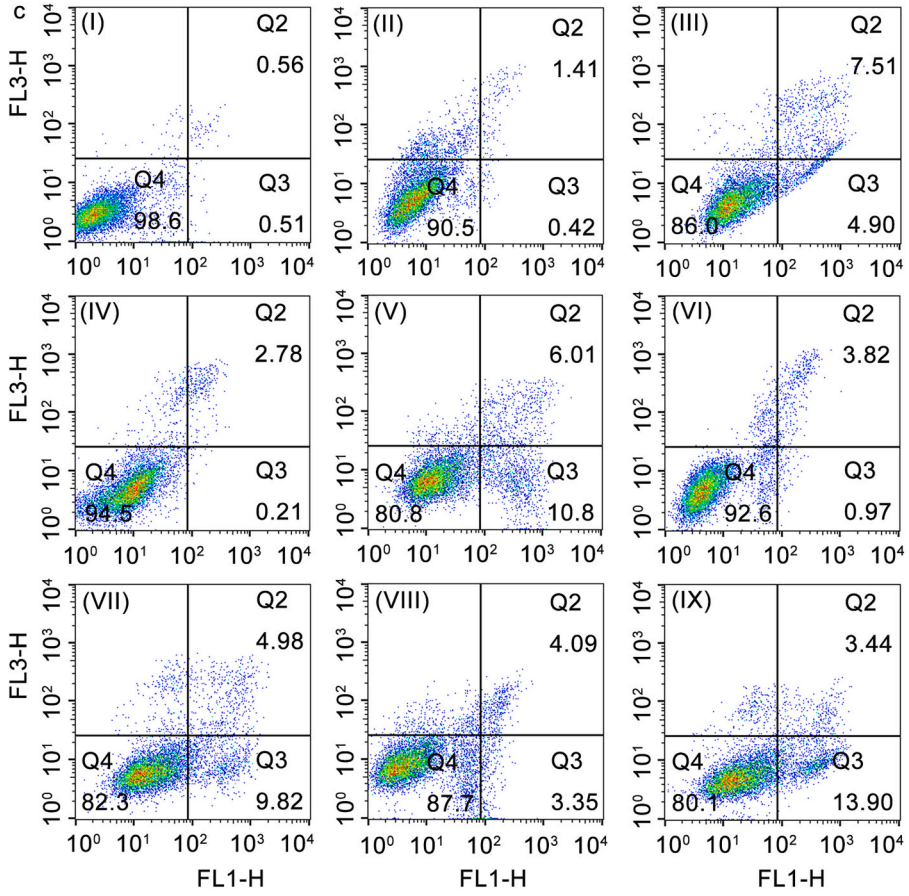

Fig. 3. (*continued*).

includes hydrogen peroxide, superoxide anion, hydroxyl radicals, etc. In this article, superoxide anion $O_2^{\bullet-}$ levels were measured with dihydroethidium (DHE) as fluorescence probe. In the presence of $O_2^{\bullet-}$, DHE can be converted to ethidium, which binds RNA or DNA to produce red fluorescence. The red fluorescence intensity is proportional to the intracellular $O_2^{\bullet-}$ levels. As shown in Fig. S7 (SI), in the control, almost no red fluorescence was observed. After SGC-7901 cells (a) were incubated with 2 × IC_{50} concentration of 4alip (b), 4alip (light, c), 4b (d), 4blip (e) and 4blip (light, f) for 24 h, distinct red fluorescence was discovered, indicating that the complexes can enhance intracellular $O_2^{\bullet-}$ levels.

Mitochondria, beyond their role in energy production, are implicated in cell differentiation, signaling, apoptosis, and cell growth and cycle regulation. They serve as integration points for signals from extrinsic and intrinsic apoptotic pathways [40,41]. Interaction of compounds with mitochondria can lead to changes in mitochondrial membrane potential. This was investigated using JC-1, a fluorescent probe emitting red or green fluorescence under high or low mitochondrial membrane potential (MMP). Fig. 3a demonstrates that 4a and 4b exhibited limited capacity to alter MMP, as indicated by the balance of red and green fluorescence points. However, a 24-h treatment of SGC-7901 cells with 4a (light), 4b (light), 4alip, 4blip, 4alip (light) and 4blip (light) resulted in decreased red and increased green fluorescence, indicating a decline in MMP.

Mitochondrial damage, a consequence of these complex interactions, can lead to a release of cytochrome C (cyto C) into the cytosol, an important apoptosis inducer. Fig. 3b shows that control and groups treated with 4a and 4b had weak green fluorescence. In contrast, the treatment of SGC-7901 cells with IC_{50} concentrations of 4a (light), 4b (light), 4alip, 4blip, 4alip (light) and 4blip (light) exhibited increased green fluorescence, which indicates an occurrence of cyto C release.

Apoptosis is a type of programmed cell demise [42]. The mitochondrial dysfunction is usually accompanied by the apoptosis. The ability of the complexes inducing cell apoptosis was investigated. See from Fig. 3c, 4a (II), 4a (light) (IV) and 4alip (VI) exhibit low apoptotic effect, 4b (III), 4b (light) (V), 4blip (VII), 4alip (light) (VIII) and 4blip (light) (IX) show high apoptotic efficacy with an apoptotic percentage of 12.41, 16.81, 14.8, 7.44 and 17.34% (early + late apoptosis), respectively. These results demonstrate that complex 4b (light), 4blip (light) reveal high anticancer activity.

The mechanism of apoptosis involves caspases, a family of proteases [43]. Western blot analysis, depicted in Fig. 3d-g, revealed that the complexes and their liposomes modulate apoptosis by altering Bcl-2 family protein expression. Specifically, they downregulated the expression of p62, caspase 3, and Bcl-2, upregulated the expression of Bax. This indicates that the complexes and their liposomal forms induce apoptosis through regulating Bcl-2 family protein.

3.5. Ferroptosis studies

As a marker of lipid peroxidation and oxidative stress, malondialdehyde (MDA) is crucial for assessing cellular oxidative stress and related disease risks. Fig. 4a shows that complex 4a has a limited ability to increase MDA levels, whereas 4b, 4a (light), 4b (light), 4alip, 4blip, 4alip (light) and 4blip (light) can effectively enhance intracellular MDA content. This indicates their potential in inducing oxidative stress within cells.

Glutathione (GSH), a key intracellular antioxidant, plays a vital role in antioxidation, protein sulfhydryl protection, and amino acid transport. The GSH to oxidized glutathione (GSSG) ratio is an essential indicator of cellular redox status. As demonstrated in Fig. 4b, treating SGC-

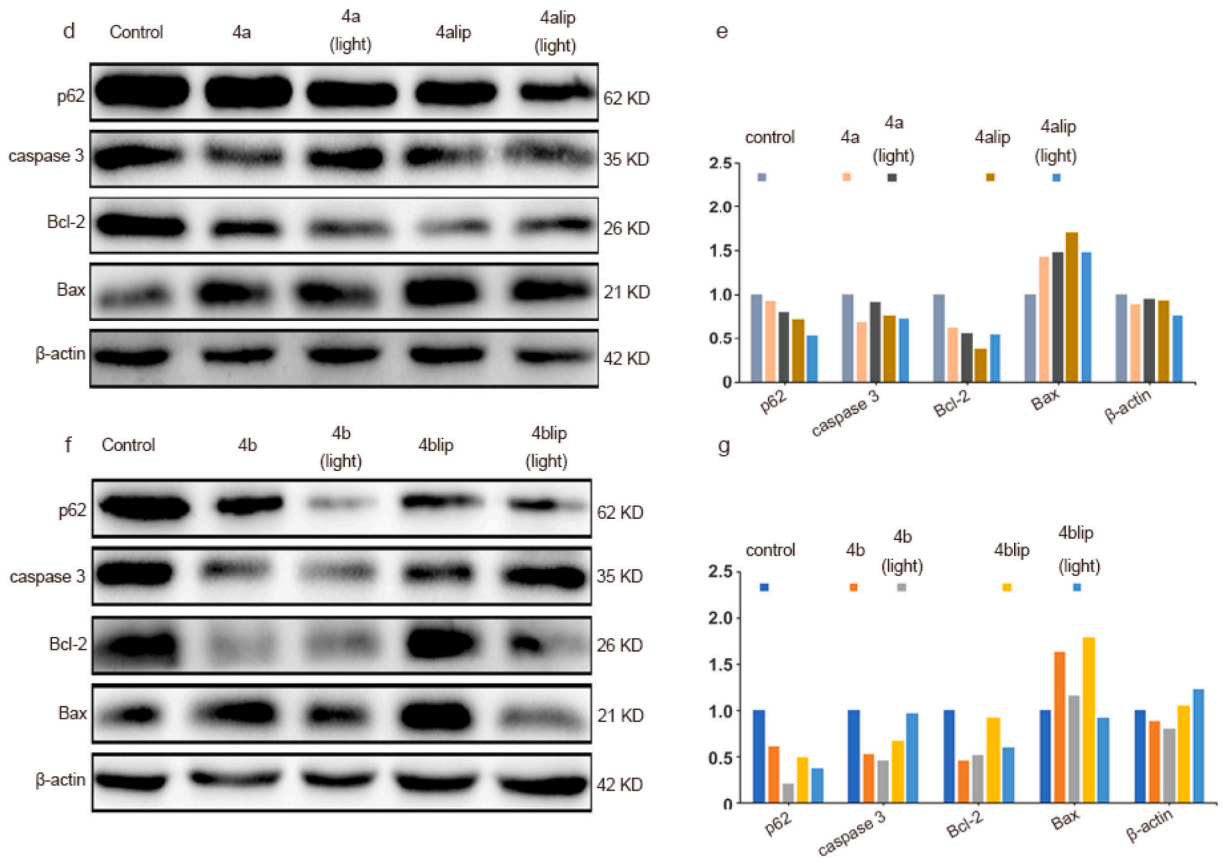

Fig. 3. (*continued*).

7901 cells with 4a (light), 4b (light), 4alip, 4blip, and 4alip (light), 4blip (light) significantly reduces intracellular GSH content and the GSH/GSSG ratio, as seen in Fig. 4c. This suggests a decrease in cellular antioxidant capacity, following the order: 4blip (light) > 4b (light) > 4alip (light) > 4alip > 4a (light) > 4b > 4a. These findings indicate that 4alip and 4blip validly hinder GSH production, promote lipid peroxidation, and consequently induce oxidative damage.

In the context of ferroptosis, an iron-dependent form of programmed cell demise different from necrosis and apoptosis, the activity of GPX4 (glutathione peroxidase 4) is an important indicator. Fig. 4d and e show that 4a, 4b, 4alip, and 4blip downregulate GPX4 protein expression, suggesting their role in inducing ferroptosis.

Lipid peroxidation, a central mechanism of ferroptosis, was examined using 4,4-difluoro-3a,4a-diaza-sindacene (C11-BODIPY). In the control and groups treated with 4a and 4b, weak green fluorescence was observed, indicating minimal lipid peroxidation (Fig. 4f). However, upon 24-h incubation of SGC-7901 cells with 4a (light), 4b (light), 4alip, 4blip, and 4alip (light), 4blip (light), an increment and a reduction in green and red fluorescence were noted, respectively. This shift signifies a transition from non-oxidized to oxidized lipids, indicating pronounced lipid peroxidation. Additionally, we also measured the cell viability induced by 4alip (light) and 4blip (light) in the presence of Fer-1, as listed in Table 2, in the presence of Fer-1, the cell viability increased compared with 4alip (light) or 4blip (light) alone. These results collectively suggest that 4a, 4b, 4alip, and 4blip can induce ferroptosis.

4. Conclusions

This study successfully prepared complexes 4a and 4b. Complex 4a demonstrated negligible cytotoxic activity, while 4b exhibited moderate cytotoxicity against selected cancer cells. Notably, upon irradiation, 4a displayed moderate and 4b showed high anticancer efficacy. Furthermore, 4a and 4b encapsulated into liposomes as 4alip and 4blip, under irradiation, significantly inhibited SGC-7901 cell proliferation. Cell colony and wound healing assays confirmed the heightened efficacy of these complexes in inhibiting cell proliferation upon irradiation. Cell cycle analysis indicated that 4alip and 4blip arrest cell growth in the S phase. Additionally, both the complexes and their liposome-loaded forms reduced mitochondrial membrane potential and triggered cytochrome *c* release, activated caspase 3, led to apoptosis by regulating and controlling the expression of Bcl-2 family proteins. Irradiation further reduced glutathione (GSH) levels and increased malondialdehyde (MDA) and lipid peroxidation, indicating ferroptosis induction by 4a, 4b, 4alip, and 4blip. Overall, this research elucidates that the complexes and their liposome-incorporated forms induce cell death via both apoptosis and ferroptosis pathways, providing valuable insights for finding newly potential anticancer candidate drugs.

Author statement

We state that the manuscript has been finished by all authors listed in the manuscript. The all data are original and real. We agree to be accountable for all aspects of the work to ensure that questions related to the accuracy or integrity of any part of the work are appropriately investigated and resolved.

All authors have read the manuscript and approved the manuscript to be submitted to JIB.

CRediT authorship contribution statement

Shuang Tian: Investigation, Methodology, Writing - original draft. **Qianying Nie:** Data curation, Software. **Haomin Chen:** Formal analysis. **Lijuan Liang:** Data curation, Methodology. **Huiyan Hu:** Formal analysis. **Shuanghui Tang:** Software. **Jiawan Yang:** Data curation.

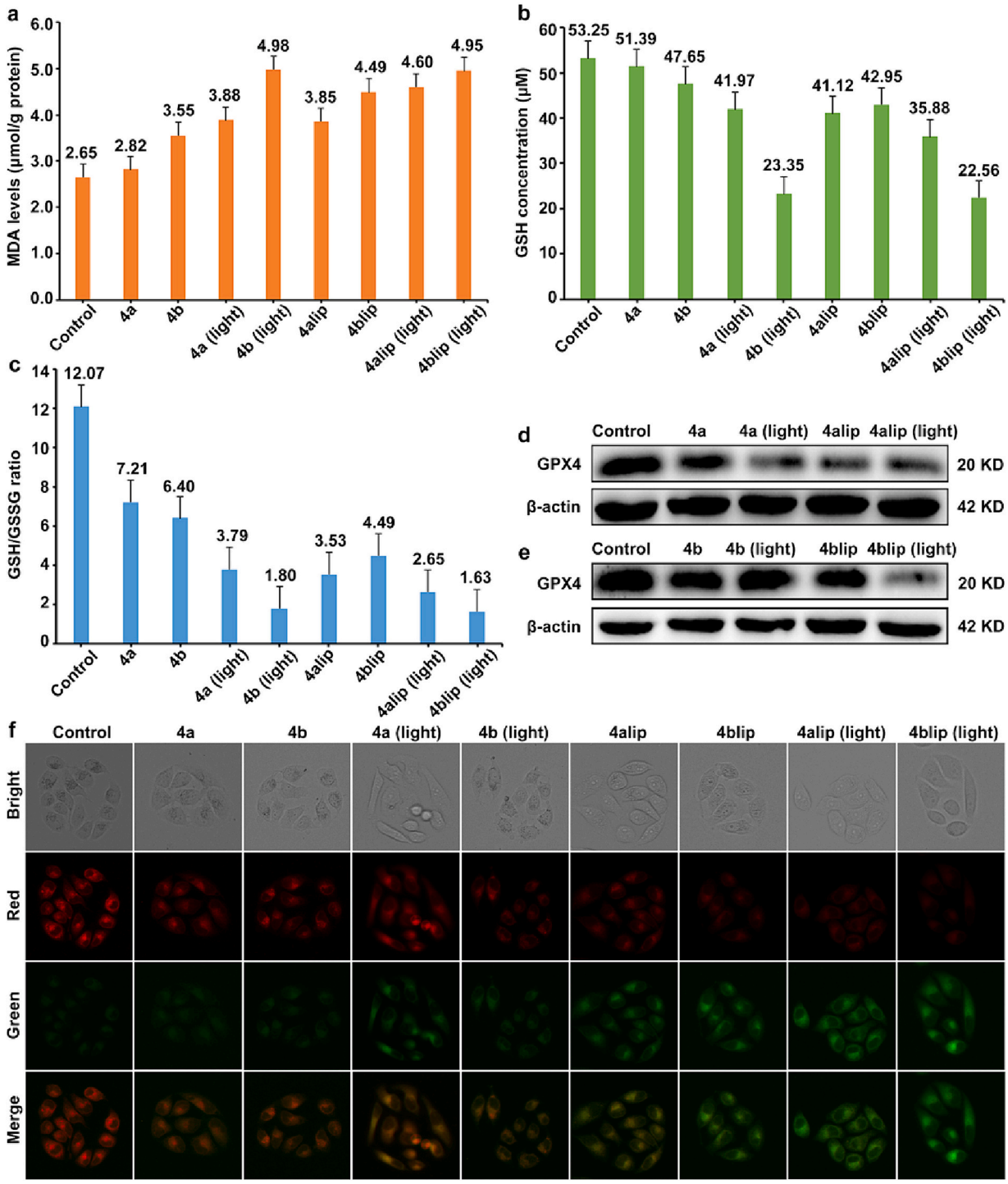

Fig. 4. Ferroptosis studies (a) MDA content, (b) GSH determination, (c) GSH/GSSG ratio, (d) and (e) expression of GPX4, (f) Assay of lipid peroxidation with C11-BODIPY-C11 after SGC-7901 cells were incubated with IC_{50} concentration of 4a, 4b, 4alip and 4blip upon irradiation or not.

Table 2
Cell viability caused by 4alip (light) and 4blip (light) in the presence of Fer-1.

		Control	4alip (light)	4blip (light)
Cell viability (%)	(−) Fer-1	100 (± 4.5)	76.2 (± 3.1)	66.8 (± 2.4)
Cell viability (%)	(+) Fer-1	99.8 (± 3.8)	94.1 (± 3.7)	87.6 (± 2.7)

Yunjun Liu: Supervision, Project administration, Conceptualization. **Hui Yin:** Conceptualization, Writing – review & editing.

Declaration of competing interest

The authors declare no competing interest exists.

Data availability

Data will be made available on request.

Acknowledgements

We are grateful for National Natural Science Foundation of China (No 21877018, 82171700).

Appendix A. Supplementary data

Supplementary data to this article can be found online at https://doi.org/10.1016/j.jinorgbio.2024.112549.

References

[1] H.H. Hartgrink, E.P.M. Jansen, N.C.T. van Grieken, C.J.H. van de Velde, Lancet. 374 (2009) 477–490.
[2] D. Wang, S.J. Lippard, Cellular processing of platinum anticancer drugs, Nat. Rev. Drug Discov. 4 (2005) 307–320.
[3] X.D. Song, X. Kong, S.F. He, J.X. Chen, J. Sun, B.B. Chen, J.W. Zhao, Z.W. Mao, Anticancer agents, Eur. J. Med. Chem. 138 (2017) 246–254.
[4] T.F. Yang, M.H. Zhu, M. Jiang, F. Yang, Z.L. Zhang, Current status of iridium-based complexes against lung cancer, Front. Pharmacol. 13 (2022) 1025544.
[5] Y.H. Yuan, Y.Y. Zhang, J. Chen, C.X. Huang, H.M. Liu, W.L. Li, L.J. Liang, Y. Wang, Y.J. Liu, Synthesis, biological evaluation of novel iridium(III) complexes targeting mitochondria toward melanoma B16 cells, Eur. J. Med. Chem. 247 (2023) 115046.
[6] H.Y. Hu, F. Zhang, Z.J. Sheng, S. Tian, G.C. Li, S.H. Tang, Y.J. Niu, J.W. Yang, Y. J. Liu, Synthesis and mitochondria-localized iridium (III) complexes induce cell death through pyroptosis and ferroptosis pathways, Eur. J. Med. Chem. 268 (2024) 116295.
[7] J. Chen, H.M. Liu, Y.C. Chen, H.Y. Hu, C.X. Huang, Y. Wang, L.J. Liang, Y.J. Liu, Iridium(III) complexes inhibit the proliferation and migration of BEL-7402 cells through the PI3K/AKT/mTOR signaling pathway, J. Inorg. Biochem. 241 (2023) 112145.
[8] Z.H. Wang, Z.X. Lv, X.C. Liu, Y.T. Wu, J.Y. Chang, R.X. Dong, C.Y. Li, X.A. Yuan, Z. Liu, Anticancer application of ferrocene appended configuration-regulated half-sandwich iridium(III) pyridine complexes, J. Inorg. Biochem. 237 (2022) 112010.
[9] G. Gupta, S. Cherukommu, G. Srinivas, S.W. Lee, S.H. Mun, J. Jung, N. Nagesh, C. Y. Lee, BODIPY-based Ru(II) and Ir(III) organometallic complexes of avobenzone, a sunscreen material: potent anticancer agents, J. Inorg. Biochem. 189 (2018) 17–29.
[10] Y. Wang, Y.Z. Li, J. Chen, H.M. Liu, Y. Zhou, C.X. Huang, L.J. Liang, Y.J. Liu, X. Z. Wang, Anticancer effect evaluation of iridium(III) complexes targeting mitochondria and endoplasmic reticulum, J. Inorg. Biochem. 239 (2023) 112054.
[11] J.J. Cao, Y. Zheng, X.W. Wu, C.P. Tan, M.H. Chen, N. Wu, L.N. Ji, Z.W. Mao, Anticancer cyclometalated iridium(III) complexes with planar ligands: mitochondrial DNA damage and metabolism disturbance, J. Med. Chem. 62 (2019) 3311–3322.
[12] W.L. Li, X.Y. Wu, H.M. Liu, C.L. Shi, Y.H. Yuan, L. Bai, X.F. Liao, Y.Y. Zhang, Y. J. Liu, Enhanced in vitro cytotoxicity and antitumor activity in vivo of iridium(III) complexes liposomes targeting endoplasmic reticulum and mitochondria, J. Inorg. Biochem. 232 (2022) 111868.
[13] X. Wang, K. Song, Y. Deng, J. Liu, Q. Peng, X. Lao, J.Y. Xu, D. Wang, T.R. Shi, Y. H. Li, D. Deng, Y.Q. Miao, Benzothiazole-decorated iridium-based nanophotosensitizers for photodynamic therapy of cancer cells, Dalton Trans. 51 (2022) 3666–3675.
[14] T. Meng, Q.P. Qin, Z.L. Chen, H.H. Zou, K. Wang, F.P. Liang, Cyclometalated Ir(III)-8-oxychinolin complexes acting as red-colored probes for specific mitochondrial imaging and anticancer drugs, Eur. J. Med. Chem. 192 (2020) 112192.
[15] I. Echevarra, E. Zafon, S. Barrabés, M.A. Martíne, S. Romas-Gómez, N. Ortega, B. R. Manzano, E.A. Jalón, R. Quesada, G. Espino, A. Massaguer, J. Inorg. Biochem. 231 (2022) 111790.
[16] X.D. Song, B.B. Chen, S.F. He, N.L. Pan, J.X. Liao, J.X. Chen, G.H. Wang, J. Sun, Guanidine-modified cyclometalated iridium(III) complexes for mitochondria-targeted imaging and photodynamic therapy, Eur. J. Med. Chem. 179 (2019) 26–37.
[17] W.L. Li, C.L. Shi, X.Y. Wu, Y.Y. Zhang, H.M. Liu, X.Z. Wang, C.X. Huang, L.J. Liang, Y.J. Liu, Light activation of iridium (III) complexes driving ROS production and DNA damage enhances anticancer activity in A549 cells, J. Inorg. Biochem. 236 (2022) 111977.
[18] A.P. Castano, T.N. Demidova, M.R. Hamblin, Mechanisms in photodynamic therapy: part one-photosensitizers, photochemistry and cellular localization, Photodiagn. Photodyn. Ther. 1 (2004) 279–293.
[19] Y.C. Chen, Y.Y. Gu, H.Y. Hu, H.M. Liu, W.L. Li, C.X. Huang, J. Chen, L.J. Liang, Y. J. Liu, Design, synthesis and biological evaluation of liposome entrapped iridium (III) complexes toward SGC-7901 cells, J. Inorg. Biochem. 241 (2023) 112134.
[20] J. Chen, W.L. Li, G.C. Li, X.M. Liu, C.X. Huang, H. Nie, L.J. Liang, Y. Wang, Y.J., Liu, targeted liposomes encapsulated iridium(III) compound greatly enhance anticancer efficacy and induce cell death via ferroptosis on HepG2 cells, Eur. J. Med. Chem. 265 (2024) 116078.
[21] C.X. Huang, Y.H. Yuan, G.C. Li, S. Tian, H.Y. Hu, J. Chen, L.J. Liang, Y. Wang, Y. J. Liu, Mitochondria-targeted iridium(III) complexes encapsulated in liposome induce cell death through ferroptosis and gasdermin-mediated pyroptosis, Eur. J. Med. Chem. 266 (2024) 116112.
[22] Y.Y. Zhang, Y. Zhou, H.W. Zhang, L. Tian, J. Hao, Y.H. Yuan, W.L. Li, Y.J. Liu, DNA-binding and evaluation of anticancer activity in vitro and in vivo of iridium (III) polypyridyl complexes, J. Inorg. Biochem. 224 (2021) 111580.
[23] S. Sprouse, K.A. King, P.J. Spellane, R.J. Watts, Photophysical effects of metal-carbon σ bonds in ortho-metallated complexes of Ir(III) and Rh(III), J. Am. Chem. Soc. 106 (1984) 6647–6653.
[24] B.L. Li, L.F. Tan, X.Q. Zou, Nucleic acid-binding comparative studies and cytotoxic properties of a Ru(II) complex, J. Iran. Chem. Soc. 9 (2012) 357–366.
[25] C. Jaafar-Maalej, R. Diab, V. Andrieu, A. Elaissari, H. Fessi, Ethanol injection method for hydrophilic and lipophilic drug-loaded liposome preparation, J. Liposome Res. 20 (2010) 228–243.
[26] X.T. Zhou, X.W. Zhang, Y.H. Ye, T.P. Zhang, H. Wang, Z.G. Ma, B.J. Wu, Nanostructured lipid carriers used for oral delivery of oridonin: an effect of ligand modification on absorption, Int. J. Pharm. 479 (2015) 391–398.
[27] L.V. Lutkus, S.S. Rickenbach, T.M. Mccormick, Singlet oxygen quantum yields determined by oxygen consumption, J. Photoch. Photobio. A. 378 (2019) 131–135.
[28] T. Mosmann, Rapid colorimetric assay for cellular growth and survival: application to proliferation and cytotoxicity assays, J. Immunol. Methods 65 (1983) 55–63.
[29] M. Kaasalainen, E. Makila, J. Riikonen, M. Kovalainen, K. Jarvinen, K.H. Herzig, V. P. Lehto, J. Salonen, Effect of isotonic solutions and peptide adsorption on zeta potential of porous silicon nanoparticle drug delivery formulations, Int. J. Pharm. 431 (2012) 230–236.
[30] W.Y. Zhang, Y.J. Wang, F. Du, M. He, Y.Y. Gu, L. Bai, L.L. Yang, Y.J. Liu, Evaluation of anticancer effect in vitro and in vivo of iridium(III) complexes on gastric carcinoma SGC-7901 cells, Eur. J. Med. Chem. 178 (2019) 401–416.
[31] M. He, Q.Y. Yi, W.Y. Zhang, L. Bai, F. Du, Y.Y. Gu, Y.J. Liu, P. Wei, Evaluation of anticancer activity in vitro and in vivo of iridium(III) polypyridyl complexes, New J. Chem. 43 (2019) 8566–8579.
[32] W.P. Fan, P. Huang, X.Y. Chen, Overcoming the achilles' heel of photodynamic therapy, Chem. Soc. Rev. 45 (2016) 6488.
[33] W.A. Velema, W. Szymanski, B.L. Feringa, Photopharmacology: beyond proof of principle, J. Am. Chem. Soc. 136 (2014) 2178.
[34] W. Lv, Z. Zhang, K.Y. Zhang, H. Yang, S. Liu, A. Xu, S. Guo, Q. Zhao, W. Huang, A mitochondri-targeted photosensitizer showing improved photodynamic therapy effects under hypoxia, Angew. Chem. Int. Ed. 55 (2016) 9947–9951.
[35] P. Zhang, H. Huang, S. Banerjee, G.J. Clarkson, C. Ge, C. Imberti, P.J. Sadler, Nucleus-targeted organoiridium–albumin conjugate for photodynamic cancer therapy, Angew. Chem. Int. Ed. 58 (2019) 2350–2354.
[36] K. Bhattacharyya, P.K. Das, Quantitative aspects of all-trans-retinol singlet and triplet quenching by oxygen, Chem. Phys. Lett. 116 (1985) 326–331.
[37] M. Miar, A. Shiroudi, K. Pourshamsian, A.R. Oliaey, F. Hatamjafari, J. Chem. Res. 45 (2021) 147–158.
[38] X.C. Liu, Z.H. Wang, X.R. Zhang, X.C. Lv, Y. Sun, R.X. Dong, G.X. Li, X.Y. Ren, Z. Y. Ji, X.A. Yuan, Z. Liu, Configurationally regulated half-sandwich iridium(III)-ferrocene heteronuclear metal complexes: potential anticancer agents, J. Inorg. Biochem. 249 (2023) 112393.
[39] B.L. Eckhardt, P.A. Francis, B.S. Parker, R.L. Anderson, Nat. Rev. Drug Discov. 11 (2012) 479–497.
[40] T.F. Chen, Y.S. Wong, Selenocystine induces apoptosis of A375 human melanoma cells by activating ROS-mediated mitochondrial pathway and p53 phosphorylation, Int. J. Biochem. Cell Biol. 41 (2009) 666–676.
[41] T.F. Chen, Y.S. Wong, Selenocystine induces apoptosis of A375 human melanoma cells by activating ROS-mediated mitochondrial pathway and p53 phosphorylation, Cell. Mol. Life Sci. 65 (2008) 2763–2775.
[42] Z. Zhang, L. Zhou, Y. Zhou, J. Liu, X. Xing, J. Zhong, G. Xu, Z. Kang, J. Liu, Mitophagy induced by nanoparticle-peptide conjugates enabling an alternative intracellular trafficking route, Biomaterials 65 (2015) 56–65.
[43] J. Li, J. Yuan, Caspases in apoptosis and beyond, Oncogene 27 (2008) 6194–6206.